Communications in Computational Chemistry
Commun. Comput. Chem., Vol. 1, No. 1, 13–23
doi: 10.4208/cicc.2025.26.01

Regular Article

Sodium Electron Solvation and Reactivity at Water Surface

Hui Dong and Yuxiang Bu*

School of Chemistry and Chemical Engineering, Shandong University, Jinan, 250010, People's Republic of China.

*Corresponding author: byx@sdu.edu.cn

Received on 26 January 2025; Accepted on 20 February 2025

Abstract

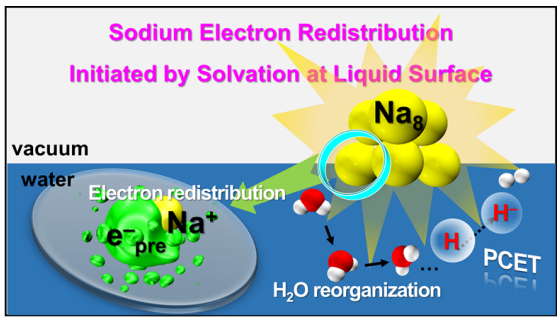

Interfacial solvated electrons (e^-_{sol}s) possess profound application values in physics, chemistry, and materials, thus attracting ever-growing attention. Although previous studies have unequivocally corroborated the involvement of e^-_{sol}s in the reaction of alkali metals with water, the mechanism has not been thoroughly revealed. Here, we simulate the solvation and ionization process of a single Na or a metallic Na_8 cluster at the vacuum-liquid interface by the hybrid functional-based *ab initio* molecular dynamics (AIMD) method, especially to elucidate the interfacial electron dynamics behavior. Results show that the electron donated by Na or Na_8 is partially solvated at the interface, a process driven by both the Na^+ interaction with the electron and its stabilization in water, which promotes electron redistribution, delocalization, and activation. Additionally, solvation increases the H_2O population near HOMO and on unoccupied orbitals, promoting H_2O reorganization and electron transfer. In aqueous solutions, Na is highly ionized and generates a unique pre-solvated electron (e^-_{pre}). Na_8 cluster, on the other hand, is partially solvated through bottom active O-coordinating sites at the interface, polarizes internally, and produces a pre-solvated dielectron ($e^{2-}_{2\ pre}$), which is followed by H_2O reorganization near the surface and the subsequent hydrogen evolution reaction by proton-coupled electron transfer. Surrounding H_2O molecules form multiple Na-O bonds with the remaining Na_8^{2+} to compensate for $e^{2-}_{2\ pre}$ loss. Our work displays the microscopic dynamics mechanism of Na and H_2O reaction by AIMD simulation and provides evidence for the participation of e^-_{pre}s in the hydrogen evolution reaction, which deepens our attention and understanding of redox reactions involving e^-_{sol}s.

Key words: Interface electron solvation, solvated electron, reactivity, proton-coupled electron transfer, *ab initio* molecular dynamics simulation.

1.Introduction

In addition to various inorganic catalytic materials [1-6], solvated electrons (e^-_{sol}), the most reducible particles in nature, play an extremely important role in many fields such as biochemistry, energy and advanced organic chemistry [7-13]. e^-_{sol}s are excess electrons with an s-like ground state formed by solvation and relaxation [14-17]. Generally, e^-_{sol}s can disintegrate the solvent structures on their first hydration layer, break chemical bonds and generate other reduction products [10, 18, 19]. At present, it has been disclosed clearly that hydrated dielectrons ($e^{2-}_{2\ aq}$s) can realize the hydrogen evolution reactions (HER) successfully

in aqueous solutions. This finding provides an intuitive dynamics process for the spontaneous HER induced by ionizing radiation and participated by e^-_{sol}s [10]. e^-_{sol}s can be generated through water decomposition by laser radiation, two-photon excitation, as well as donation by photoelectron donors represented by I^- and CN^- and other pathways [7, 20-25]. However, the ionization of alkali metals represented by sodium is one of the main means to produce e^-_{sol}s in both homogeneous and heterogeneous systems [26-28]. Besides, the gas-phase deposition with Na atoms as neutral precursors can ionize them at the liquid surface, and then release e^-_{sol}s into solutions [29]. With the help of gas-phase deposition and molecular beam methods, Gilbert M. Nathanson's group has carried out extensive researches on reduction reactions induced by e^-_{sol}s at the gas-liquid interface, such as Benzyltrimethylammonium and glycerol [26, 30-32]. Their studies establish a strategy to explore near-interfacial analogs of radical chemistry in aqueous solutions by evaporating intermediates into gas phase, and also provide information support and method guidance for the mechanism speculation and exploration of the chemical reactions involved e^-_{sol}s at the gas-liquid interface and near surface.

Electron transfer (ET) at the solid-liquid interface is of great research value in physics and chemistry, especially in electrochemistry [33-39]. Although the accurate detection of ET information has been allowed by the current development of experimental techniques, it is still necessary to describe ultrafast electron behaviors on picosecond or even femtosecond timescales [38, 40-43]. Studies on ET at the solid-liquid interface focus on photocatalysts/H_2O, oxides/H_2O, semiconductor materials/H_2O in photochemical reactions or Cu/H_2O, Fe/H_2O, Au/H_2O interface and others [33, 35, 43-49]. Generally, the wide band gap oxides such as TiO_2, SiO2, MgO can be illuminated to excite electrons that are located at the valence band to relax into the water conduction band, then, ET is realized between two phases. Simultaneously, OH^-, H_2 and e^-_{sol} form at the interface [33, 50, 51]. As the typical electron donor, the research on Na atoms is limited to the static calculation or dynamics simulation of a single Na atom in small and medium-sized water clusters or at the liquid surface to characterize its electronic structure [26, 30, 52-58]. With the rapid development of technology means, recent experimental studies have been able to capture the formation process of e^-_{sol}s in the reaction of metallic Na with H_2O accurately [59]. The relationship between e^-_{sol} and Na^+ in aqueous solutions and the reactive intermediates in Na and H_2O reactions have also been elucidated and speculated by Car-Parrinello molecular dynamics (CPMD) simulation [60-63]. Unfortunately, although e^-_{sol}s have been verified in the reaction of Na and H_2O [59], the Na electronic structure and electron rearrangement before ET between two phases remains an unknown "black box", which has seriously retarded the explanation of classical Na-H_2O reaction mechanism. Therefore, the study of ET behavior at Na/H_2O interface is necessary.

Moreover, according to Marcus theory, solvent reorganization in solution including molecular structure and orientation changes will significantly influence the ET rate [34, 64]. In the process of ET at the solid-liquid interface, H_2Os solvation is the critical factor. And the successful ET will act on interfacial structures in turn [34, 48, 65, 66]. So the study on synchronous changes of the interfacial structure and electron behavior during the ET process at the solid-liquid interface is important to understand electron transfer mechanism and solvation effect.

In this work, referring to existing experimental and theoretical studies [30, 59, 62, 63], we explore the solvation process of the monomeric Na and Na_8 metallic cluster at the vacuum-liquid interface and in aqueous solutions, and also describe the specific interfacial electron dynamics behavior by ab initio molecular dynamics (AIMD) simulation. Our study uncovers that both Na and Na_8 HOMO electrons can be partially solvated, redistributed, delocalized and destabilized because of the Pauli repulsion between Na valence electron and O lone pair electron, and also be turned into e^-_{pre} and $e^{2-}_{2\,pre}$, respectively. More importantly, solvation increases the H_2O population near HOMO and on the orbitals to be occupied, boosting H_2O reorganization and ET. Consequently, HER initiated by Na_8 $e^{2-}_{2\,pre}$ occurs with H and H^- anion as intermediates through proton-coupled ET (PCET). Due to multiple Na atoms existence and Na solvation, we conclude that the Na clusters represented by Na_8 are all capable of being pre-solvated and inducing H_2O recombination near the water surface. This study clarifies the electron behavior and reaction mechanism for Na and H_2O reactions and also provides a theoretical basis for the HER involving e^-_{pre}s.

2. Simulation details

In this study, the reason why we choose Na atom and a Na_8 cluster as the research objects is shown in the Supporting Information (SI). Since Na_8 has eight Na atoms with a T_d symmetric structure and a low-energy nondegenerate a1 and higher triply degenerate t1 molecular orbitals, it is necessary to reveal the solvation process, phenomenon and results of a single Na atom at the vacuum-liquid interface first. We hope that single Na solvation could provide preliminary information for subsequent studies on Na_8 solvation with more complex geometry variation and molecular orbital evolution information.

We first constructed a periodic box containing 64 H_2Os with a vacuum length of 15 Å. After a long enough time of pre-equilibrium, a periodic representative system with a volume of $12.53\times27.53\times12.53$ $Å^3$ was extracted. Then, one Na atom or a Na_8 (T_d) metallic cluster was added at 3.4 Å above the water surface, and initial velocities were set as -0.05 Å/fs, that is, make them move towards the water surface (Figure 1) [26, 52].

AIMD simulations under the unrestricted open-shell were carried out by using the CP2K/Quickstep software package [67, 68] At present, the PBEh40 functional has been widely applied in the research field of e^-_{sol}s (Details on the reasons for choosing the PBEh40 functional are provided in the section of **Computational details** in the SI) [10, 33, 54, 69-72]. Therefore, all simulations were done by employing the PBE functional with 40% Fock exchange components [73, 74] and introducing a non-local rVV10 scheme (b=5.3,C=0.0093) to describe van der Waals (vdW) interaction [73, 75, 76]. The core electrons of each element are described by the Goedecker-Teter-Hutter (GTH) mode-conserving pseudopotentials [77] and the valence electrons are described by the Gaussian mixed plane wave basis set (GPW) [77]. The Kohn-Sham (KS) orbital is expanded into a TZVP-type Gaussian basis set, and the electron density is truncated to a plane wave basis set of 300 Ry [78]. At the same time, the auxiliary density matrix method (ADMM) based on the cFIT3 auxiliary basis set [79] is used to effectively reduce the computational resource consumption. The dynamics simulations were performed with a time step of 0.5 fs, and the temperature was controlled at 350 K utilizing a canonical (NVT) ensemble and a CSVR thermostat [80].

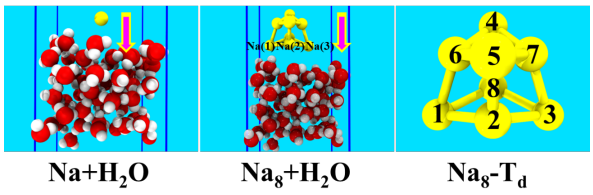

Figure 1. The initial configuration of AIMD simulations and the specific atomic numbers of Na_8 (to make as many Na atoms as possible touch the water surface at the same time to simulate the real reaction between a multi-atomic cluster and H_2O, the Na_8 (T_d) orientation was fined-tuned during constructing the initial configuration, so that the plane formed by three Na atoms at the front bottom was basically parallel to the surface and they were designated as Na(1), Na(2) and Na(3) from left to right. The magenta arrows point to the motion directions of Na and Na_8, and the blue line is the periodic box boundary).

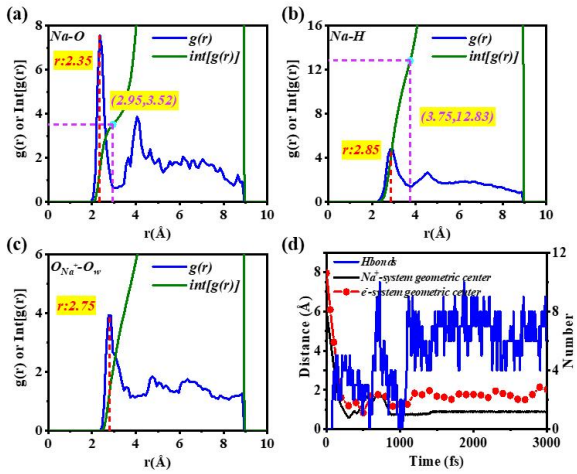

Figure 2. Solvation of single Na atom. (a, b) Radial distribution functions (RDF) and their integral function curves of the number of O and H around Na in the AIMD simulation trajectory. (c) RDF and its integral function curve of $O_{Na}{}^{+}$-O_w ($O_{Na}{}^{+}$: the O atom within 3 Å of Na, the distance (3 Å) is determined according to the first O coordination layer of Na atom shown by the RDF integral function curve; O_w: the O atom of H_2O). (d) Distances of Na^+ core or the Na valence electron from the system geometric center versus time in the simulation. Besides, the time evolution of the number of hydrogen bonds ($O_{Na}{}^{+}$-H_w) between H_2O within 3 Å of Na atom and its surrounding H_2Os. $O_dH_d\cdots O_a$ (d: donor, a: acceptor) pairs are considered as hydrogen bonds if the angle $\angle H_dO_dO_a \leq 35$ and the distance $O_d\cdots O_a \leq 3$Å .

The subsequent studies and analyses were carried out based on the AIMD trajectories and each frame configuration in the dynamic trajectories was read.

Firstly, to obtain the energy level of the water phase during the dynamics process, we extract the configurations from the trajectories except Na or Na_8 cluster and carry out single point calculations on them. Secondly, since the Na_8 highest occupied molecular orbital (HOMO) is difficult to be separated when mixed into the conduction band of the aqueous solvent phase, additional single-point calculations by quantum mechanics/molecular mechanics (QMMM) method are performed in addition to AIMD to characterize the HOMO energy level changes on Na_8 cluster in the dynamics trajectory. Na_8 cluster and all other H_2Os are retained in the QM and MM subsystems, respectively. The cubic periodicity as well as the cell size of the original system are completely inherited in the QM and MM regions. In the QM part, the hybrid functional and parameter settings are the same as those in the AIMD simulation. The MM part is described by SPC/E classical force field [81], and the coupling between QM and MM part is solved by density-derived atomic charge [81] and multiple grid method [82]. The Na_8 HOMO energy level obtained under QM/MM theory is used as its frontier molecular orbitals energy level in AIMD simulation. In addition, vertical ionization potential (VIP) is calculated at PBEh40/TZVP (800 Ry) level in CP2K. The density of states (DOS) and spectroscopies of selected snapshots from the MD trajectory are obtained by Multiwfn [83]. And the electron density diagrams in the paper are all assisted by VMD software [84]. The simulation results with other initial structures are placed in the SI.

3.Results and discussion

Solvation and ionization process of Na and Na_8 at water surface

Solvation of single Na atom. The Na atom impinges on the water surface at an initial velocity of 0.05 Å/fs. After about 50 fs, the Na atom can reach the surface and be pre-solvated (Figure S1). In the following time, the Na atom continues being partially solvated by H_2Os and is embeded below the surface, as does the valence electron (e^-_{val}) (Figure 2d and S1).

From 0 to 1000 fs, the number of hydrogen bonds formed between $O_{Na}{}^{+}$ (the O atoms within 3Å of Na^+) and other H2Os decreases and fluctuates drastically (Figure 2d). After 1000 fs, the number of hydrogen bonds ($O_{Na}{}^{+}$-H_w) increases (Figure 2d). And the $O_{Na}{}^{+}$-O_w RDF shows a peak at $\sim$ 2.8 Å (Figure 2c), which is also the typical O-O distance in liquid water, [85, 86] suggesting that the hydrogen-bonding network is destroyed by Na collision and Na pre-solvation is reconstructed at the surface. The O atom/H atom closest to Na is distributed at a distance of 2.35 Å/2.85 Å [87], and Na is 2.95 Å/3.75 Å away from its first O/H coordination layer (Figure 2a, b). This is exactly consistent with the average number of O atoms within 3 Å distance from Na atom in the dynamics trajectory obtained by our statistics (Figure 4a). The result also indicates that the solvated Na adopts the Na···O rather than Na···H coordination mode, which is consistent with the basic structure of a hydrated Na extracted from the AIMD simulation trajectory (Figure 3e).

As Na moves perpendicular to the surface at a given initial velocity and continues to evolve, five representative solvated Na atomic states have been extracted from the dynamics simulation trajectory (Figure 3) [88]. Initially, a dipole-bound surface state appears by dangling O-H bonds from H_2Os on the surface (Figure 3a). Subsequently, H_2Os on one side provide dangling O-H bonds and hydrogen bond network to stabilize e^-_{pre}, while H_2Os on the other side begin to adjust direction for coordinating with Na^+.

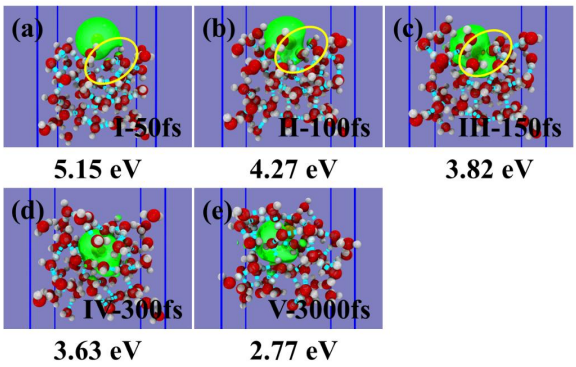

Figure 3. The five representative states of Na solvation in the AIMD simulation trajectory (the spin density isosurface is 0.0004 and the cyan cylinder lines are hydrogen bonds formed by H_2Os). The data marked below are VIP values of the corresponding structures at each time [52]. (a) A dipole-bound surface state, (b) a proper surface state, (c) a partially embedded state, (d) a cavity state, (e) a highly ionized state, forming a tightly bound cation-electron pair, (Na^+_{sol} : e^-_{pre}).

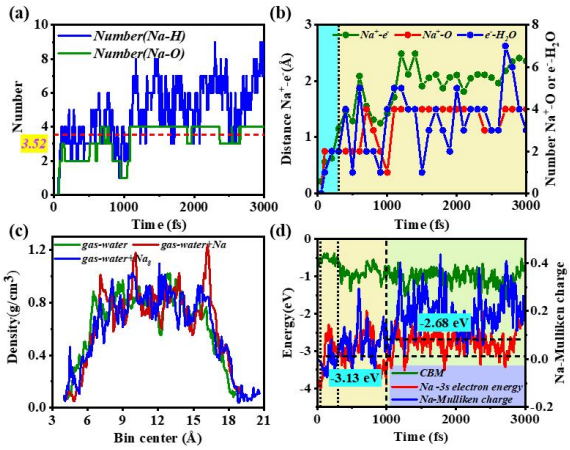

Figure 4. Solvation of single Na atom. (a) Evolution of the number of atoms within the distance of 3 Å from Na atom and the statistics are carried out at intervals of 5 fs. The dotted line represents the average number of Na-O coordination bonds in the full dynamics trajectory. (b) Evolution of the distance between Na^+ and the Wannier orbital center of the Na valence electron (Na^+-e^-), the number of O within the distance of 3 Å from Na^+ (Na^+-O) and the number of H_2O molecules within the distance of 3 Å from the Wannier orbital center of Na valence electron (e^--H_2O) over time. The number statistics are based on the point of 100 fs interval within 3000 fs. The position marked by the dotted line is at 300 fs. (c) H_2O density distribution along the surface normal for the aqueous interface with pure water, Na-contained and Na_8-contained trajectories (H_2O mass is replaced by O atom mass). The bottom boundary of the periodic box is at y = 0 (Figure 1). (d) Evolution of the energy levels of water conduction band bottom (CBM) and the Na valence electron (e^-_{val}), and the Na Mulliken charge over time. The positions marked by the first and the second dotted lines are at 50 fs and 300 fs, respectively. The dashed lines are the energy levels of a solvated electron (-3.13 eV)[17] and Na e^-_{val} (-2.68 eV, the average energy level after 1000 fs), respectively.

The formation of semi-cavity at the surface makes it possible for the transient Na half-cavity surface state (Figure 3b). Then, H_2O timely orientation on one side facilitates the Na^+-O formation. With the help of the dangling O-H bonds offered by H_2Os, e^-_{pre} localizes to a partially embedded surface state (Figure 3c) and Na atom with reduced VIP continues to be solvated below the water surface (Figure 3d, e). The transformation between these states and electron localization is possibly attributed to the location of dangling O-H bonds and the reconfiguration of hydrogen-bonding network among solvents. Due to the Pauli repulsion interaction with lone pair electrons in O of H_2O, Na valence electron deviates in the opposite Na^+-O direction (Figure 3 and Figure 4b) and then occupies the anti-orbitals of O and H (Figure 5a). Thus, it breaks the hydrogen bonds between the occupied H atoms with other nearby H_2Os, which forms a cavity and further intensifies the high-density localization distribution of the excess electron in weak or missing hydrogen bond regions [18]. The representative configuration (Figure 3e) obtained by the AIMD simulation trajectory accords with the basic structure of the hydrated Na atom already mentioned in the literature, that is e^-_{aq}: Na^+ contact pair [52, 61].

In the middle and late stages of this simulation (after 1000 fs), the distance between e^-_{val} (Wannier orbital center, WOC) and Na^+ increases and oscillates within the range of 2.0-2.5 Å (Figure 4b). At the same time, the number of Na^+-O coordination bonds increases and stabilizes at 4 (Figure 4a). The e^-_{val} is solvated by 4 H_2Os (Figure 4b). Besides, we also find a correlation between the excess electron hydration degree and the Na^+-e^- distance. This is manifested in the fact that the fluctuation trends of Number(e-H_2O) and Distance (Na^+-e^-) are synchronized, either increasing or decreasing (Figure 4b). The former is driven and determined by the electrostatic attraction between the positive Na^+ core and e^-_{val}, and coordination between Na^+ and H_2O. The electrostatic attraction between the positive Na^+ and e^-_{val} tends to maintain the original intact neutral atomic structure. However, studies have previously shown that H_2O or glycerol reorientation is not only necessary to promote Na ionization, but also vital for stabilizing positive/negative products [26, 29, 52]. Because the solvation for Na electron weakens the attractive interaction between the excess electron and Na^+, and also strengthens the Na^+ coordination with H_2Os, the distance of Na^+ and e^- at 3000 fs (structure V, Figure 3e) becomes longer than that of them initially (Figure 4b). There is still an approximate energy difference of 2 eV between the conduction band bottom (CBM) of the water phase and the e^-_{val} energy level (Figure 4d). This large energy difference cannot be compensated or erased by Na solvation directly and simply. For another, the average Na Mulliken charge is only 0.2 (Figure 4d) and the e^-_{val} is within 3 Å of Na^+ (Figure 4b), indicating that the electron is just partially solvated. Nevertheless, with the rapid solvation process and time evolution, the electron transforms from a valence state attached to Na^+ core to a pre-solvated electronic state in water, forming a highly ionized Na atom or a tight cation electron pair (Na^+_{sol}:e^-_{pre}) [54, 60, 61]. The VIP of the electron

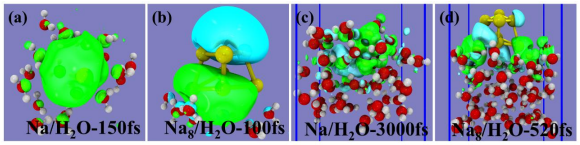

Figure 5. (a, b) The representative snapshots of pre-solvated electrons extracted from the AIMD trajectories of Na/H_2O and Na_8/H_2O, showing the occupation of the pre-solvated electrons on O and H atoms (a: the top view spin density isosurface of 0.0004. b: the α HOMO electron isosurface, cyan/green isovalue is 0.01/-0.01). (c, d) The charge density difference (cyan/green isosurface: 0.0005/-0.0005, electron accumulation/consumption) of Na/H_2O and Na_8/H_2O.

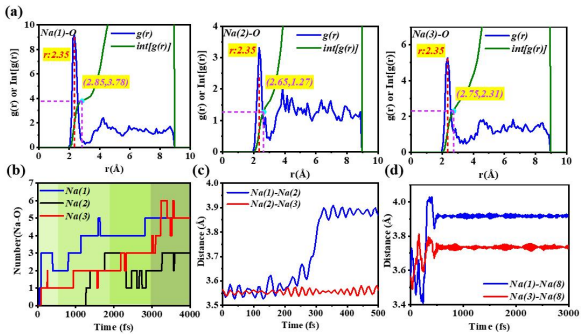

Figure 6. (a) The radial distribution functions (RDF (Na, O)) and their integral functions of the number of O around three Na atoms (Na(1), Na(2) and Na(3)) closest to the water surface on the Na_8 cluster in the AIMD simulation trajectory, respectively. (b) Evolution of the number of O around the three Na atoms over time (Number (Na-O)). The number statistics are based on the number of atoms within the distance of 3 Å from Na atom and are carried out at intervals of 5 fs. The regions with different background colors are divided by three important time points (525 fs, 1900 fs and 2955 fs) in the HER process. (c) Evolution of the bond lengths between Na(1) and Na(2), Na(2) and Na(3) over time. (d) Evolution of the bond lengths between Na(1) and Na(8), Na(3) and Na(8) over time.

attached Na atom on the water surface is 5.15 eV. However, the distance between Na^+ and e^-_{pre} in Na^+_{sol}:e^-_{pre} increases to 2.357 Å and the VIP value can be greatly reduced to 2.77 eV (Figure 3e and 4b).

It is suggested that the e^-_{val} is destabilized into the weakly bound e^-_{val} through solvation and gets a higher energy level than that of e^-_{sol} in the bulk liquid water band gap (Figure 4d), which explains its remarkable activity at the interface. We still hope to realize HER under the influence of $e^{2-}_{2\,aq}$ or multiple Na atoms solvation effect. Then, a small-sized Na_8 cluster solvation process and phenomenon are studied, and H_2O dissociation and HER are observed successfully.

Solvation of Na_8 cluster. After adding other substances, especially Na_8 to the water surface, the H_2O density distribution along the surface normal shows a much lower degree of structured order, a sharper peak near the surface and a wider distribution range. Furthermore, its maximum and minimum values fluctuate much more and the peak shifts backward (Figure 4c) [54]. Therefore, compared with the interface without Na or Na_8, H_2Os move more rapidly and disorderedly, facilitating the following electron solvation and transfer.

The hydration structure of three Na atoms at the bottom of the Na_8 cluster, namely Na(1), Na(2) and Na(3), is investigated in the same way as a single Na atom discussed above. The RDF results show that the positions of O atoms closest to Na(1), Na(2) and Na(3) are all 2.35 Å (Figure 6a), which consists with the single metal Na solvation in water (Figure 2a). However, because the solvent environment and positions of these three Na atoms are different, there is still obvious disparateness in their hydration structures. And the solvation degree and speed of Na(1) and Na(3) at Na_8 apex are significantly higher than those of Na(2) in Na_8 middle, which are also verified by orbital-weighted Fukui functions (Figure S3). But Na(2) only starts its solvation at 1270 fs, which occurs after the loss of $e^-_{pre}(1)$ (a Na_{8sol} HOMO α electron) via PCET (525 fs) in HER (Figure 6b). According to this dynamics trajectory, similar to the single Na solvation, Na(1) and Na(3) on Na_8 bottom vertex become active reaction sites to coordinate with H_2Os (Figure 6b). As a consequence, the sequential solvation on these three bottom Na atoms for Na_8 renders its obvious internal electron polarization (Figure S4a). What's more, given that Na(1) and Na(3) are positioned at Na_8 bottom vertices (the closest to water surface) and the Na(1)-O and Na(3)-O bonds form almost simultaneously (Figure 6b), it is reasonable to assume that their solvation processes commence nearly synchronously. They can transfer partial negative charges to other Na atoms before $e^-_{pre}(1)$ transfers to solutions (at 525 fs), e.g., Na(2) and Na(8), which occupy less-favorable solvation sites, during the period of 0 to 525 fs (Figure S4a, b). Na(1) solvation elongates the bond length of Na(1)-Na (neighboring Na atoms of Na(1) on Na_8), as does Na(3) (Figure 6c,d). After $e^-_{pre}(1)$ loss, Na atoms of Na_8+ which is close to the surface form more Na-O bonds to stabilize the positive cluster (Figure S4c and S5b).

After losing $e^-_{pre}(2)$ (a Na_{8sol} HOMO β electron), the remaining $Na_8{}^{2+}$ solvation is more intense. After $e^-_{sol}(2)$ departure (nearly 2000 fs), the much more Na-O-Na bridge bond formation (Figure S5c) manifests that $Na_8{}^{2+}$ balances its positive charges through subsequent solvation. Meanwhile, the Na-O bond length (Figure S4c,d) is the same as the RDF obtained by solvation analysis of Na on Na_8 (Figure 2a and 6a). Only from the perspective of geometric configuration, $Na_8{}^{2+}$ undergoes deformation seriously after losing $e^-_{pre}(1)$ and $e^-_{pre}(2)$. Apart from the solvated Na(1), Na(2) and Na(3) exhibiting electropositivity, some positive charges of $Na_8{}^{2+}$ also gather on Na(5), while others accumulate negative charges or retain a neutral structure (Figure S4a,b, Table S2). Na(6) and Na(7) are located at unfavorable solvation positions, while Na(5) is in an advantageous position on Na_8 and Na(8) is closer to the surface than it (Figure 1). Therefore, after $e^-_{pre}(2)$ loss (nearly 2000 fs), partial electron transfer occurs from Na(5) and Na(8) to Na(6) and Na(7) (Figure S4b). Force-field molecular dynamics (FFMD) simulations have shown that the remaining positive Na clusters are surrounded by hydroxide anions [59]. So once $Na_8{}^{2+}$ forms, it has fallen into the surface water environment, H_2Os solvate it timely and bond to these five Na with significant positive charges at cluster bottom and outer edge, including Na(1), Na(2), Na(3), Na(5) and Na(8) (Figure S5c). Na_8 evolution at the vacuum-liquid interface suggests that

Na(1) removes slightly from the cluster and tends to be solvated as $Na^+(1)$ (Figure 6c,d). After $e^-_{pre}(1)$ is released into water and combines with $H^+(1)$ by PCET, there is much more serious Na^+_{8sol} electron polarization which is displayed on Na(1), Na(2) and Na(3) (Figure S4a). Subsequently, after $e^-_{pre}(2)$ also enters the aqueous solution to participate in $H^-(1)$ formation (at 1895 fs), the remaining Na^{2+}_{8sol} solvation and its internal electron polarization are significantly intensified, which is prominently manifested in Na(5), Na(6), Na(7) and Na(8) (Figure S4b). Due to internal electron polarization and electrostatic repulsion between ionized Na, the result shows that the positive cluster which releases two e^-_{pre}s tends to dissociate. Meanwhile, the electron polarization and charge imbalance observed among Na atoms and caused by varying solvation environments (Figure S4a, b), along with the alteration in Na_8 total charge (gradually increasing from 0 to 1 and ultimately reaching 2, Table S1), serve as compelling evidence that the two e^-_{pre}s transferred sequentially from Na_8 to the aqueous solution are not contributed solely by a specific Na atom.

The proton quantum effects alter the interaction patterns between H_2O and Na^+, thereby enhancing the ionic mobility [89, 90]. The classical model tends to over-estimate the rigidity of hydration structures. In contrast, fully quantum-mechanical calculations can notably reduce the solvation free energy of Na^+ in aqueous solutions by roughly 10-20 % [91, 92]. This allows H_2Os to adjust their distribution around solutes rapidly. The results show that Na/Na_8 with an initial velocity of 3.4 Å/fs can reach the water surface in a short time and promptly initiate the solvation process. Specifically, at merely 100 fs, a nearby H_2O (within a range of 3 Å) solvates Na valence electron, and simultaneously, two Na^+-O bonds are formed (Figure 4b). At just 50 fs, Na_8 can form a single Na^+-O bond with H_2O (Figure 6b). Additionally, the energy level of the Na 3s electron increases instantaneously, indicating that the electron is activated (Figure 4d). These imply that the surrounding H_2O molecules can respond rapidly to the solute. Meanwhile, from 1085 fs until the end of the dynamic trajectory at 3000 fs, a stable number (3-4) of Na^+-O bonds are formed by Na^+ with the surrounding H_2Os (Figure 4a), which demonstrates the stability of the solvation structure. However, as Na_8 continuously releases e^-_{pre}s into the aqueous solution, the number of Na^+-O bonds on it increases steadily (Figure 6b, Figure S4c, d). On the other hand, the solvation effect leads to an increase in the distance between Na^+ and e^-, from 0.214 Å (at 0 fs) to 0.561 Å (at 100 fs). It takes only 300 fs for the distance to exceed 1 Å (1.156 Å, Figure 4b). Moreover, the fluctuation range of the Na Mulliken charge subsequently expands and exhibits positive values (Figure 4d), suggesting that the rapid adjustment of the solvation structure (Figure 3) promotes the charge transfer from solutes to solvents.

In short, we elucidate the solvation and ionization processes of Na and Na_8 at the water surface through AIMD simulations, uncovering the changes in their electronic properties and geometric structures. Firstly, Na undergoes pre-solvation induced by the Pauli repulsion from the lone pair electrons of O in H_2O. It is highly ionized and produces e^-_{pre}. Secondly, Na(1) and Na(3), positioned at the vertices of Na_8, are in the most favorable solvation sites. Due to the diverse solvation environments experienced by each individual Na atom, the varying degrees of solvation among them lead to internal electron polarization in Na_8. This polarization phenomenon becomes more pronounced following the e^-_{pre}s transfer into aqueous solutions. Compared with previous studies on finite-size $(H_2O)_n$ clusters, through constructing a large-scale aqueous solution environment, we illustrate the evolution of the structures and properties of metal atoms and clusters more intuitively and comprehensively.

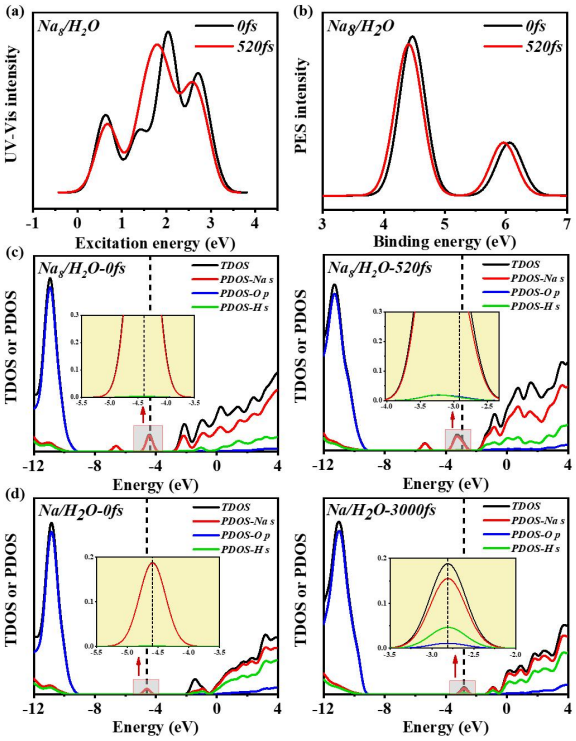

Figure 7. The UV-Vis (a) and Na_8 PES (b) spectrums of Na_8/H_2O. The DOS plots of Na s in Na and Na_8, O p and H s of H_2O in Na/H_2O (c) and Na_8/H_2O (d), respectively.

Electron redistribution affected by Na solvation.

It is apparently revealed that Na exhibits strong interaction with O of H_2O, which thus promotes significantly the electron redistribution shown by charge density difference diagrams (Figure 5c, d). Although HER in the aqueous solution can't be induced by a single Na solvation, the Na valence electron deviates from Na^+ to water and exhibits a more destabilized state (Figure 5c), which is consistent with the conclusion of our investigation on Na solvation that a highly ionized Na is obtained by solvating (Figure 3e).

According to the dynamics trajectory, the Na_8 electrons transfer into the aqueous solution to participate in the HER by PCET after 520 fs (Figure S9), so we focus on Na_8 electron structure and its electron distribution in the period from 0 fs to 520 fs. Due to the Na^+-O bond formation, Na_8 electrons delocalize from the two active O-coordinating sites near the surface (Figure 5d), which agrees with the results that partial electron transfer occurs from middle Na(5) and Na(8) to the outer edge Na(6) and Na(7) (Figure S4b). Accordingly, Na_8 breaks T_d symmetry. Its HOMO electrons are stabilized by polar H-O bonds and repelled inward by Pauli repulsion with lone pairs of O and also penetrate the surface and the near-surface layer (Figure S5a and S9). Compared with the UV-Vis spectrum at 0 fs, the Na_8/H_2O adsorption peak redshifts and strength decreases at 520 fs, also

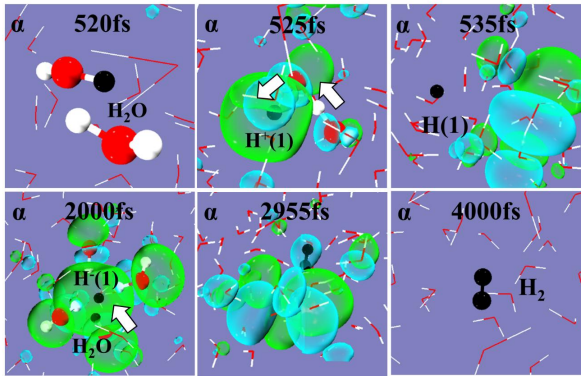

Figure 8. The H_2 formation process. H_2O dissociation and H^+ neutralization (R1), anionization (R2) and H_2 formation (R3) in aqueous solution during the Na_8 solvation-induced hydrogen evolution reaction (the cyan HOMO isosurface is 0.01 and green -0.01). The figure shows α-HOMO that omits its occupation on Na_8. At 520 fs, α-HOMO all occupies Na_8. At 525 fs, a large proportion of it still occupies Na_8, except for a small proportion in $H^+(1)$ as shown. Before $H^-(1)$ formation, β-HOMO always occupies Na_8. After 2000 fs, α and β become a closed-shell (CS) state so we only show α occupation here. At the end of our dynamics simulation (4000 fs), α-HOMO and β-HOMO both occupy in the aqueous solution after H_2 formation. Specific HOMO occupation is shown in Figure S9.

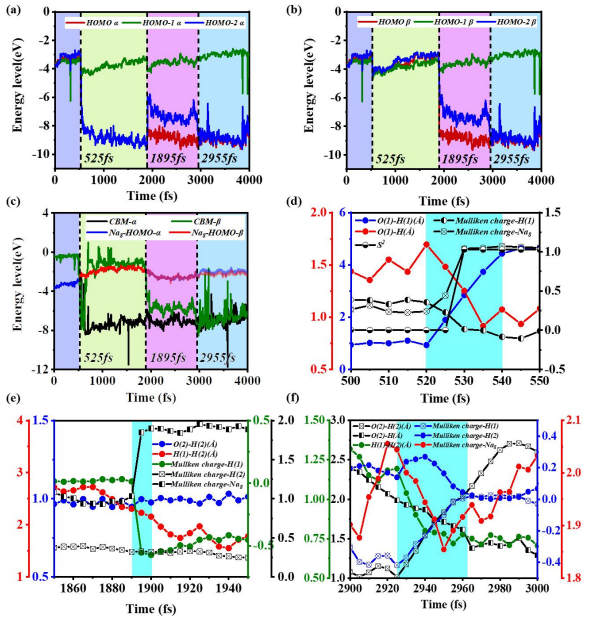

Figure 9. (a, b) Time evolutions of energy levels of Na_8. (c) Evolution of the water conduction band bottom (CBM-α, CBM-β) and the HOMO energy levels of the Na_8 cluster (Na_8-HOMO-α, Na_8-HOMO-β) calculated by QM/MM theory over time. Among them, we should pay attention to the α-HOMO (Na-HOM-α) and β-HOMO (Na-HOM-β) energy levels of Na_8 cluster during 0-520 fs and 525-1900 fs, respectively. In the AIMD simulation, both α-electron and β-electron in Na_8 HOMO have entered the aqueous solution, so we pay no attention to them after 1900 fs. (d) With cooperative Na_8 solvation and its neutralization (R1), both breaking and formation of the $H^+(1)$ dissociated from H_2O, the Mulliken charges of atoms and the spin square $< S^2 >$ of the system with time (500-550 fs). (e) $H^-(1)$ formation by binding $e^-_{sol}(2)$ (R2) (1850-1950 fs). (f) Evolution of interatomic distances and Mulliken charges over time (2900-3000 fs) during the reaction (R3) for H_2 formation.

indicating that Na_8 electron state is changed (Figure 7a). This is consistent with the result that delocalized electrons are formed by Na_8 solvation. And the Na_8 AIP value at 520 fs (3.475 eV) is lower than that at 0 fs (3.858 eV) (Table S3). It is worth highlighting that before electron transfer, the spin-paired double electrons on Na_8 HOMO have been following the CS state evolution as a partially or pre-solvated dielectron ($e^{2-}_{2\,pre}$). The adsorption peak with weaker strength in PES spectrums shifts to a lower energy region (Figure 7b). The eight Na 3s electrons form four orbitals including a triply degenerate HOMO and HOMO-1, therefore, there are only two distinct peaks shown in DOS (Figure 7d). Notably, the electrons are activated and DOS presents a higher HOMO energy level at 3000 fs or 520 fs (Figure 7c,d), demonstrating Na oxidation and facilitating electron transfer into solutions. Compared with the specific configurations at 0 fs, DOS suggests that the energy gaps are narrowed at 3000 fs and 520 fs for Na/H_2O and Na_8/H_2O, respectively. Moreover, after solvating, H_2Os, especially H s orbitals, get a higher population near the HOMO and the orbitals to be occupied, indicating it is potential to be occupied by Na or Na_8 electrons.

In short, there is a strong interaction between Na and the O in H_2O, which significantly promotes electron redistribution. Consequently, the electrons can be pre-solvated, then partially delocalized into aqueous solutions and activated. Here, based on the research of single alkali metal atoms, we further explore the solvation process of metal clusters. In many previous studies on e^-_{sol}s, the scenario of adding a metal block, which means adding multiple single metal atoms simultaneously, has rarely been thoroughly considered. Our research indicates that although the solvation outcomes of single metal atoms are representative, the solvation and electron redistribution processes of metal clusters are intricately associated with the solvation environment of each atom within the clusters.

Hydrogen evolution reaction of Na with H_2O.

H_2 production induced by Na ionization at the liquid surface, such as glycerol, has been experimentally demonstrated [30]. According to previous experimental and theoretical studies, the HER is triggered successfully through an $e^{2-}_{2\,aq}$ rather than a single e^-_{aq} in aqueous solutions [10, 93]. However, a partially solvated e^-_{pre} can only be provided by a single Na atom in Na/H_2O, while the partially solvated $e^{2-}_{2\,pre}$ is offered by Na_8 HOMO in Na_8/H_2O. The HER initiated by Na_8 solvation is divided into four reaction steps (R1-R4, Figure 8). Three important time points are involved, which are 525 fs, 1900 fs and 2955 fs. The first hydrogen proton ($H^+(1)$) is dissociated from H_2O by cooperative Na_8 solvation and its rapid neutralization ($H^-(1)$, R1) by PCET. $H^-(1)$ is anionized ($H^-(1)$, R2) by the electron provided by Na^+_{8sol} in the same way and H_2 forms (R3). Immediately, $[Na_8(OH_{(3)})]^+$ formation occurs (R4). In the reaction (R1-R4), the most noteworthy process is the

H_2O dissociation triggered by Na_8 solvation. We will discuss them detailedly in the following text.

R1: $Na_{8sol}\left(\text{or } Na^+_{8sol} + e^-_{pre}(1)\right) + H_2O_{(1)} \longrightarrow Na^+_{8sol} + H_{(1)} + OH^-_{(1)}$,
(PECT or cooperative H_2O dissociation and Na_8 solvation (ionization).)

R2: $H_{(1)} + Na^+_{8sol}\left(\text{or } Na^{2+}_{8sol} + e^-_{(2)}\right) \rightarrow H^-_{aq(1)} + Na^{2+}_{8sol}$,

R3: $H^-_{aq(1)} + H_2O_{(2)} \rightarrow H_2 + OH^-_{(2)}$,

R4: $Na^{2+}_{8sol} + OH^-_{(2)} + H_2O_{(3)} \rightarrow \left[Na_8(OH_{(3)})\right]^+ + H_2O$.

Prior to electron transfer, similar to Na, Na_8 double HOMO electrons are pre-solvated and delocalized and also occupy the anti-orbitals of O and H on H_2Os (Figure 5b, S5a and S9), which weakens the O-H bond strength and accelerates proton transfer in water. A short proton transfer reaction has already happened in an aqueous solution to reorganize H_2O molecules (Figure S6), which provides the basis for the subsequent easy H_2O dissociation [94].

Solvent recombination is followed by PCET and the dissociated H_2O is located on the adjacent region of Na_8 $e^{2-}_{2\ pre}$ (Figure 8). Na_8 significant solvation activates its electrons and leads to the energy-level splitting of its degenerate orbitals (HOMO, HOMO-1, HOMO-2, Figure 9a,b), and H_2O recombination weakens the O-H bond. Firstly, $e^-_{pre}(1)$ and $e^-_{pre}(2)$ can easily span a distance of about 6 Å and both partially distribute on $H_2O(1)$, which greatly breaks the O-H bond to 1.9 Å (Figure S9, Table S1). Meanwhile, the energy levels of the orbitals occupied by both α and β electrons decrease. Specifically, the energy levels of the α-HOMO and α-(HOMO-2) orbitals significantly decrease to approximately the water valence band (-9.29 eV, Figure 9a,b). The water CBM energy level decreases at this moment (at 525 fs) and it crosses the HOMO energy level of Na_8 cluster (Na_8-HOMO-α, Na_8-HOMO-β, Figure 9c). Electrons can transfer freely between Na_8 and the aqueous solution without an energy barrier, which provides the basis for a rapid proton neutralization reaction (R1). Subsequently, under the influence of the electrostatic attraction from the proton ($H^+(1)$) in the aqueous phase without energy obstruction, electron resonance happens between the aqueous solution and Na_8. The pre-solvated electrons ($e^-_{pre}(1)$, $e^-_{pre}(2)$) on the Na_8 cluster are partially and directly bound to $H^+(1)$ in solution by a long-distance jumping mechanism (525-530 fs) (Figure 9d). Immediately after $H^+(1)$ dissociates, $e^-_{pre}(1)$ transfers to solutions but $e^-_{pre}(2)$ returns to Na_8 HOMO completely and forms Na^+_{8sol}. The water CBM (CBM-α, CBM-β) shows a symmetry-broken (BS) state evolution (Figure 9c and S9) and the CBM-β level re-elevates but slightly below its original level (-0.54 eV) after an extremely brief reduction (Figure 9c). From 520 fs, the consistency between the O(1)-$H^-(1)$ distance, the Mulliken charge of Na_8 and $H^-(1)$ indicates the cooperative reaction of H_2O dissociation and Na_8 ionization and HER starts as the proton-coupled electron transfer. It takes only 10 fs for the proton ($H^+(1)$) to complete the neutralization process after separating from H_2O and harvesting the Na_8 electron ($e^-_{pre}(1)$, R1) (Figure 9d,e). Additionally, the production of H atoms is monitored and verified by Mass spectroscopy and TOF distribution in HER occurred at the vacuum-glycerol interface [26, 29, 30, 95]. As the proton ($H^+(1)$) is lost, the remaining OH spreads away through hydrogen bond network in aqueous solution. After $e^-_{pre}(1)$ leaves Na_8 and binds to $H^+(1)$, an intermediate process of BS appears. $e^-_{pre}(2)$ still binds to Na^{2+}_{8sol} and doesn't enter the aqueous solution directly with $H^-(1)$ to form H at the same time (Figure S9).

After a neutral H(1) atom forms as the reaction intermediate 1 (R1), it is necessary to find a favorable hydration environment for combining $e^-_{pre}(2)$ to form the new and important $H^-(1)$ intermediate (R2, Figure 9e). Since its formation, it gradually moves about 5-6 Å distance from interior water toward surface and is located near Na^+_{8sol} finally (Figure S5d,e). The orbital energy of Na^+_{8sol} β electron also mixes with the water CBM-β (Figure 9c), removing the energy barrier for the successful $e^-_{pre}(2)$ transfer to $H^-(1)$ subsequently. Na_8 continues to provide $e^-_{pre}(2)$ (R2) in a long-distance jumping way for $H^-(1)$ which is 4 Å away (Figure S8f and S9). The energy levels of its β-HOMO and β-(HOMO-2) orbitals decrease substantially and respectively exhibit a CS state with the α-HOMO and α-(HOMO-2) orbitals (Figure 9a, b). H^- has been speculated as the intermediate of HER initiated through two e^-_{aq}s by optical transient absorption and electron paramagnetic resonance (EPR) experimentally, and confirmed to be involved in HER triggered by $e^{2-}_{2\ aq}$ [10, 96, 97].

$H^-(1)$ attracts surrounding H_2O molecules to provide hanging O-H bonds for stability (Figure 8 and S8e). The gap between water CBM-α and CBM-β receiving $e^-_{pre}(2)$ is still more than 1.0 eV (Figure 9c). Influenced by the speed of hydration structure adjustment, $H^-(1)$ exists stably for about 1000 fs in this dynamics simulation (Figure S8c). H_2 is formed (R3) by $H^-(1)$ with $H^+(2)$ offered by the H_2O in $H^-(1)$ first hydration layer (Figure 8 and 9f) and remains stable until the end of our simulation. Until the HER is completed at 2955 fs, except for the fact that the HOMO-1 remains at a relatively high energy level, the energy levels of HOMO and HOMO-2 remain consistent and low (Figure 9a, b). It is worth pointing out that the H_2Os contributing to $H^-(1)$ stabilization by hanging O-H bond include the one that coordinates to Na at Na_8 vertex (labeled as H_2O-vertex, Figure S7b). Surprisingly, $H^+(2)$ is not supplied by H_2O-vertex but by another H_2O in the proton transfer step (R3). Therefore, NaOH and H_2 are not produced synchronously and the remaining $OH^-(2)$ diffuses away through the hydrogen bond network in an aqueous solution. After losing $e^-_{pre}(2)$ (at 1895 fs), Na^{2+}_{8sol} is stable and solvated by surrounding solvents until the highly solvated Na^+ at Na^{2+}_{8sol} vertex binds OH after H_2O recombination and generates $[Na_8(OH)]^+$ (R4, Figure S7c). Transient $[Na_8(OH)]^+$ formation has been observed in our dynamics trajectories but only exists for about 300 fs (3920-4220 fs, Figure S7e). Although this OH leaves Na^{2+}_{8sol} , Na^{2+}_{8sol} doesn't dissociate and retains its original solvation structure.

In short, we determine the reaction steps of HER initiated by the Na_8 solvation. The HER occurs as Na_8 donates two e^-_{pre}s to the aqueous solution. This process proceeds via the PCET mechanism with H and H^- as intermediates. Generally, the H-O bond in the H_2O molecule exhibits a bond energy of approximately 464 kJ/mol, rendering it challenging to break directly. In this study, the results of the spontaneous processes, including H_2Os recombination, PCET and HER, are consistent with the existing conclusion that proton quantum effects offer a low-energy-barrier pathway for proton transfer [98, 99]. This part of the study provides theoretical evidence for the experimentally verified conclusion that the HER in aqueous solutions is triggered

by $e_{2\ aq}^{2-}$ rather than e_{aq}^{-}. Moreover, it clarifies the specific reaction mechanism and electron behavior during the generation of e_{sol}^{-}s, the initiation, and the completion of the HER in the Na-H_2O reaction. It proves that e_{sol}^{-}s are essential reducing agents in this reaction.

4. Conclusion

In this work, referring to previous studies, we carry out the solvation process of a single metallic Na atom and the Na_8 cluster at the interface by employing AIMD method, focusing on revealing the interfacial electron dynamics behavior triggered by Na solvation. We propose that the electrons donated by Na atoms are activated and redistributed through solvation. Furthermore, the H_2O population is increased under the solvation effect near HOMO and on the orbitals to be occupied. Concretely, Na goes into the water surface to be ionized heavily and generates a partially e_{pre}^{-}. For the small-sized Na_8 cluster located at the vacuum-liquid interface, it is also capable of being partially solvated through the active O-coordinating sites located at the bottom vertex. And Na_8 HOMO $e_{2\ pre}^{2-}$ generated by solvation embeds the near-surface layer and occupies the anti-bond orbitals of O and H, prompting H_2O reorganization near the surface. H^+ can be dissociated easily and neutralized by PCET, and the subsequent HER proceeds successfully with H and H^- as crucial intermediates. After two e_{pre}^{-}s are released into an aqueous solution, much more Na-O bonds form to balance the accumulated positive charges. This work will provide detailed microdynamics information for Na and H_2O reactions and contribute further understanding to the redox reactions involving e_{sol}^{-}s.

Supporting Information

The following supporting information can be downloaded at:
https://global-sci.com/storage/self-storage/cicc-2025-26-1-r1-si.pdf

Electron morphology diagrams of a single Na solvation; Na_8 solvation and hydrogen evolution reaction (R1–R4); Na_8 solvation and hydrogen evolution reaction (R1–R4) simulated by *ab initio* molecular dynamics with a different initial configuration (Na_8/H_2O); Na_8 solvation and hydrogen evolution reaction (R1–R4) simulated by *ab initio* molecular dynamics with different Na_8 orientation and water-box (Na_8/H_2O).

References

[1] Yang C., Cui Y., Cheng Y., Su Y., Yao D., Chen G., Song K., Liu S., Fang Y., Wu Y., Song Y., Lu G., Li Z., Boosting photocatalytic hydrogen evolution activity by accelerating water dissociation over $Rh/Zn(OH)_2$ catalyst in alkaline solution, *ACS Appl. Energy Mater.*, **6** (2023), 10180–10189

[2] Wu Y., Wang L., Bo T., Chai Z., Gibson J.K., Shi W., Boosting hydrogen evolution in neutral medium by accelerating water dissociation with Ru clusters loaded on MO_2CT_x MXene, *Adv. Funct. Mater.*, **33** (2023), 2214375

[3] Wilson J.C., Caratzoulas S., Vlachos D.G., Yan Y., Insights into solvent and surface charge effects on Volmer-step kinetics on Pt (111), *Nat. Commun.*, **14** (2023), 2384

[4] Bender J.T., Petersen A.S., Østergaard F.C., Wood M.A., Heffernan S.M.J., Milliron D.J., Rossmeisl J., Resasco J., Understanding cation effects on the hydrogen evolution reaction, *ACS Energy Lett.*, **8** (2023), 657–665

[5] Cheng J., Niu Z., Zhao Z., Pei X., Zhang S., Wang H., Li D., Guo Z., Enhanced ion/electron migration and sodium storage driven by different MoS_2–$ZnIn_2S_4$ heterointerfaces, *Adv. Energy Mater.*, **13** (2023), 2203248

[6] Li L., Wang P., Shao Q., Huang X., Metallic nanostructures with low dimensionality for electrochemical water splitting, *Chem. Soc. Rev.*, **49** (2020), 3072–3106

[7] Grills D.C., Lymar S.V., Solvated electron in acetonitrile: radiation yield, absorption spectrum, and equilibrium between cavity- and solvent-localized states, *J. Phys. Chem. B*, **126** (2022), 262–269

[8] Ding Z.T., Guo Z., Zheng Y., Wang Z., Fu Q., Liu Z., Radiotherapy reduces N-oxides for prodrug activation in tumours, *J. Am. Chem. Soc.*, **144** (2022), 9458–9464

[9] Huang S., Gao L., Fu Q., Bu Y.X., Regulating work function of $[Ca24Al28O_{64}]^{4+}$:$4e^-$ electrides via changing solvated-electron characters, *J. Phys. Chem. Lett.*, **12** (2021), 3274–3280

[10] Gao L., Zhang L., Fu Q., Bu Y.X., Molecular-dynamics characterisation of dielectron hydration in liquid water with unique double-proton transfers, *J. Chem. Theory Comput.*, **17** (2021), 666–677

[11] Anstoter C.S., DelloStritto M., Klein M.L., Matsika S., Modelling the ultrafast electron-attachment dynamics of solvated uracil, *J. Phys. Chem. A*, **125** (2021), 6995–7003

[12] Ou H.H., Tang C., Chen X.R., Zhou M., Wang X.C., Solvated electrons for photochemistry syntheses using conjugated carbon-nitride polymers, *ACS Catal.*, **9** (2019), 2949–2955

[13] Wu S.Q., Xue L.J., Bu Y.X., Unique solvated-electron state and its remarkable enhancement effect on internuclear J-couplings in fluorocarbon cage electron clathrates, *J. Phys. Chem. C*, **126** (2022), 4965–4974

[14] Glover W.J., Schwartz B.J., The fluxional nature of the hydrated electron: energy and entropy contributions to aqueous-electron free energies, *J. Chem. Theory Comput.*, **16** (2020), 1263–1270

[15] Ariyarathna I.R., Pawlowski F., Ortiz J.V., Miliordos E., Aufbau principle for diffuse electrons of double-shell metal–ammonia complexes: the case of $M(NH_3)_4$@$12NH_3$, M = Li, Be^+, B^{2+}, *J. Phys. Chem. A*, **124** (2020), 505–512

[16] Pizzochero M., Ambrosio F., Pasquarello A., Picture of the wet electron: a localised transient state in liquid water, *Chem. Sci.*, **10** (2019), 7442–7448

[17] Ambrosio F., Miceli G., Pasquarello A., Electronic levels of excess electrons in liquid water, *J. Phys. Chem. Lett.*, **8** (2017), 2055–2059

[18] Iglev H., Kolev S.K., Rossmadl H., Petkov P.St., Vayssilov G.N., Hydrogen-atom transfer from water or alcohols activated by presolvated electrons, *J. Phys. Chem. Lett.*, **6** (2015), 986–992

[19] Christianson J.R., Zhu D., Hamers R.J., Schmidt J.R., Mechanism of N_2 reduction to NH_3 by aqueous solvated electrons, *J. Phys. Chem. B*, **118** (2014), 195–203

[20] Novelli F., Chen K., Buchmann A., Ockelmann T., Hoberg C., Head-Gordon T., Havenith M., The birth and evolution of solvated electrons in water, *Proc. Natl. Acad. Sci.*, **120** (2023), e2216480120

[21] Hartweg S., Barnes J., Yoder B.L., Garcia G.A., Nahon L., Miliordos E., Signorell R., Solvated dielectrons from optical excitation: an effective source of low-energy electrons, *Science*, **380** (2023), 1161–1165

[22] Bachman B.F., Zhu D., Bandy J., Zhang L., Hamers R.J., Detection of aqueous solvated electrons produced by photoemission from solids using transient-absorption measurements, *ACS Meas. Sci. Au*, **2** (2022), 46–56

[23] Bragg A.E., Schwartz B.J., The ultrafast charge-transfer-to-solvent dynamics of iodide in tetrahydrofuran. 1. Exploring the roles of solvent and solute electronic structure in condensed-phase charge-transfer reactions, *J. Phys. Chem. B*, **112** (2008), 483–494

[24] Zhu D.T., Zhang L., Ruther R.E., Hamers R.J., Photo-illuminated diamond as a solid-state source of solvated electrons

in water for nitrogen reduction, *Nat. Mater.*, **12** (2013), 836–841

[25] Zhang L., Zhu D., Nathanson G.M., Hamers R.J., Selective photoelectrochemical reduction of aqueous CO_2 to CO by solvated electrons, *Angew. Chem. Int. Ed.*, **53** (2014), 9746–9750

[26] Wiens J.P., Nathanson G.M., Alexander W.A., Minton T.K., Lakshmi S., Schatz G.C., Collisions of sodium atoms with liquid glycerol: insights into solvation and ionisation, *J. Am. Chem. Soc.*, **136** (2014), 3065–3074

[27] Bragg A.E., Cavanagh M.C., Schwartz B.J., Linear-response breakdown in solvation dynamics induced by atomic electron-transfer reactions, *Science*, **321** (2008), 1817–1827

[28] Weyl W., Ueber Metallammonium-Verbindungen, *Ann. Phys.*, **197** (1864), 601–612

[29] Tesa-Serrate M.A., Smoll E.J., Minton T.K., McKendrick K.G., Atomic and molecular collisions at liquid surfaces, *Annu. Rev. Phys. Chem.*, **67** (2016), 515–540

[30] Alexander W.A., Wiens J.P., Minton T.K., Nathanson G.M., Reactions of solvated electrons initiated by sodium-atom ionisation at the vacuum–liquid interface, *Science*, **335** (2012), 1072–1075

[31] Gao X.F., Hood D.J., Zhao X., Nathanson G.M., Creation and reaction of solvated electrons at and near the surface of water, *J. Am. Chem. Soc.*, **145** (2023), 10987–10990

[32] Gao X.F., Nathanson G.M., Exploring gas–liquid reactions with microjets: lessons we are learning, *Acc. Chem. Res.*, **55** (2022), 3294–3302

[33] Ding Z.T., Goldsmith Z.K., Selloni A., Pathways for electron transfer at MgO–water interfaces from *ab initio* molecular dynamics, *J. Am. Chem. Soc.*, **144** (2022), 2002–2009

[34] Zwaschka G., Lapointe F., Campen R.K., Tong Y., Characterisation of ultrafast processes at metal/solution interfaces: towards femtoelectrochemistry, *Curr. Opin. Electrochem.*, **29** (2021), 100813

[35] Acharya S., Lancaster M., Maldonado S., Semiconductor ultramicroelectrodes: platforms for studying charge-transfer processes at semiconductor/liquid interfaces, *Anal. Chem.*, **90** (2018), 12261–12269

[36] Migani A., Blancafort L., Excitonic interfacial proton-coupled electron-transfer mechanism in the photocatalytic oxidation of methanol to formaldehyde on TiO_2(110), *J. Am. Chem. Soc.*, **138** (2016), 16165–16173

[37] Chu W., Saidi W.A., Zheng Q., Xie Y., Lan Z., Prezhdo O.V., Petek H., Zhao J., Ultrafast dynamics of photogenerated holes at a CH_3OH/TiO_2 rutile interface, *J. Am. Chem. Soc.*, **138** (2016), 13740–13749

[38] Muller E.A., Strader M.L., Johns J.E., Yang A., Caplins B.W., Shearer A.J., Suich D.E., Harris C.B., Femtosecond electron solvation at the ionic-liquid/metal-electrode interface, *J. Am. Chem. Soc.*, **135** (2013), 10646–10653

[39] Selcuk S., Selloni A., Facet-dependent trapping and dynamics of excess electrons at anatase TiO_2 surfaces and aqueous interfaces, *Nat. Mater.*, **15** (2016), 1107–1112

[40] Sulpizi M., Salanne M., Sprik M., Gaigeot M.P., Vibrational sum-frequency-generation spectroscopy of the water liquid–vapour interface from density-functional-theory-based molecular-dynamics simulations, *J. Phys. Chem. Lett.*, **4** (2013), 83–87

[41] Grunder Y., Lucas C.A., Probing the charge distribution at the electrochemical interface, *Phys. Chem. Chem. Phys.*, **19** (2017), 8416–8422

[42] Matsuzaki K., Kusaka R., Nihonyanagi S., Yamaguchi S., Nagata T., Tahara T., Partially hydrated electrons at the air/water interface observed by UV-excited time-resolved heterodyne-detected vibrational sum-frequency-generation spectroscopy, *J. Am. Chem. Soc.*, **138** (2016), 7551–7557

[43] Stahler J., Deinert J.C., Wegkamp D., Hagen S., Wolf M., Real-time measurement of the vertical binding energy during the birth of a solvated electron, *J. Am. Chem. Soc.*, **137** (2015), 3520–3524

[44] Lapointe F., Wolf M., Campen R.K., Tong Y., Probing the birth and ultrafast dynamics of hydrated electrons at the gold/liquid-water interface via an optoelectronic approach, *J. Am. Chem. Soc.*, **142** (2020), 18619–18627

[45] Santos J.C.C., Negreiros F.R., Pedroza L.S., Dalpian G.M., Miranda P.B., Interaction of water with the gypsum (010) surface: structure and dynamics from nonlinear vibrational spectroscopy and *ab initio* molecular dynamics, *J. Am. Chem. Soc.*, **140** (2018), 17141–17152

[46] Meyer M., Bertin M., Bovensiepen U., Wegkamp D., Krenz M., Wolf M., Ultrafast dynamics at the $Na/D_2O/Cu(111)$ interface: electron solvation in ice layers and Na^+-mediated surface solvation, *J. Phys. Chem. C*, **115** (2011), 204–209

[47] Fischer S.A., Duncan W.R., Prezhdo O.V., *Ab initio* non-adiabatic molecular dynamics of wet electrons on the TiO_2 surface, *J. Am. Chem. Soc.*, **131** (2009), 15483–15491

[48] Iida K., Role of hydration in photoexcited electron transfer between a gold nanocluster and a water molecule, *J. Phys. Chem. C*, **126** (2022), 7492–7499

[49] Rego L.G., Batista V.S., Quantum-dynamics simulations of interfacial electron transfer in sensitised TiO_2 semiconductors, *J. Am. Chem. Soc.*, **125** (2003), 7989–7997

[50] Le Ca"er S., Water radiolysis: influence of oxide surfaces on H_2 production under ionising radiation, *Water*, **3** (2011), 235–253

[51] Chelnokov E., Cuba V., Simeone D., Guigner J.M., Schmidhammer U., Mostafavi M., Le Ca"er S., Electron transfer at oxide/water interfaces induced by ionising radiation, *J. Phys. Chem. C*, **118** (2014), 7865–7873

[52] Cwiklik L., Buck U., Kulig W., Kubisiak P., Jungwirth P., A sodium atom in a large water cluster: electron delocalisation and infrared spectra, *J. Chem. Phys.*, **128** (2008), 154306

[53] Wiens J.P., Alexander W.A., Sodium-atom beam collisions with the liquid-glycerol surface: mass effects of deuteration, *Chem. Phys. Lett.*, **730** (2019), 321–325

[54] Ding Z.T., Selloni A., Electron trapping and ion leaching at the Li-modified quartz–water interface, *J. Phys. Chem. C*, **124** (2020), 26741–26747

[55] Dierking C.W., Zurheide F., Zeuch T., Med J., Parez S., Slav'iček P., Revealing isomerism in sodium–water clusters: photoionisation spectra of $Na(H_2O)_n$ (n = 2–90), *J. Chem. Phys.*, **146** (2017), 244303

[56] Forck R.M., Dauster I., Schieweck Y., Zeuch T., Buck U., Onč'ak M., Slav'iček P., Observation of two classes of isomers of hydrated electrons in sodium–water clusters, *J. Chem. Phys.*, **132** (2010), 221102

[57] Meng S., Gao S., Formation and interaction of hydrated alkali-metal ions at the graphite–water interface, *J. Chem. Phys.*, **125** (2006), 014708

[58] Carnevali S., Proust C., Soucille M., Unsteady aspects of sodium–water–air reaction, *Chem. Eng. Res. Des.*, **91** (2013), 633–639

[59] Mason P.E., Uhlig F., Vanek V., Buttersack T., Bauerecker S., Jungwirth P., Coulomb explosion during the early stages of the reaction of alkali metals with water, *Nat. Chem.*, **7** (2015), 250–254

[60] Park S.J., Narvaez W.A., Schwartz B.J., *Ab initio* studies of hydrated-electron/cation contact pairs: hydrated electrons simulated with density-functional theory are too kosmotropic, *J. Phys. Chem. Lett.*, **14** (2023), 559–566

[61] Park S.J., Narvaez W.A., Schwartz B.J., How water–ion interactions control the formation of hydrated-electron:sodium-cation contact pairs, *J. Phys. Chem. B*, **125** (2021), 13027–13040

[62] Mundy C.J., Hutter J., Parrinello M., Microsolvation and chemical reactivity of sodium and water clusters, *J. Am. Chem. Soc.*, **122** (2000), 4837–4838

[63] Mercuri F., Mundy C.J., Parrinello M., Formation of a reactive intermediate in molecular-beam chemistry of sodium and water, *J. Phys. Chem. A*, **105** (2001), 8423–8427

[64] Marcus R.A., Chemical and electrochemical electron-transfer theory, *Annu. Rev. Phys. Chem.*, **15** (1964), 155–196

[65] Kılıç M., Ensing B., Microscopic picture of the solvent reorganisation during electron transfer to flavin in water, *J. Phys. Chem. B*, **123** (2019), 9751–9761

[66] Verma P., Ghosh D., Dutta A.K., Electron attachment to cytosine: the role of water, *J. Phys. Chem. A*, **125** (2021), 4683–4694

[67] Kuhne T.D., Iannuzzi M., Del Ben M., Rybkin V.V., Seewald P., Stein F., Laino T., Khaliullin R.Z., Schutt O., Schiffmann F., Golze D., Wilhelm J., Chulkov S., Bani-Hashemian M.H., Weber V., Borstnik U., Taillefumier M., Jakobovits A., Lazzaro A.S., Pabst H., Muller T., Schade R., Guidon M., Andermatt S., Holmberg N., Schenter G.K., Hehn A., Bussy A., Belleflamme F., Tabacchi G., Gloss A., Lass M., Bethune I., Mundy C.J., Plessl C., Watkins M., VandeVondele J., Krack M., Hutter J., CP2K: an electronic-structure and molecular-dynamics software package—Quickstep: efficient and accurate electronic-structure calculations, *J. Chem. Phys.*, **152** (2020), 194103

[68] VandeVondele J., Krack M., Mohamed F., Parrinello M., Chassaing T., Hutter J., Quickstep: fast and accurate density-functional calculations using a mixed Gaussian and plane-waves approach, *Comput. Phys. Commun.*, **167** (2005), 103–128

[69] Gao L., Bu Y.X., Competitive hydration versus migration of pre-hydrated electrons for CO_2 reduction in aqueous solution revealed by *ab initio* molecular-dynamics simulation, *Adv. Theory Simul.*, **6** (2023), 2200938

[70] Lan J.G., Chergui M., Pasquarello A., Dynamics of the charge transfer to solvent process in aqueous iodide, *Nat. Commun.*, **15** (2024), 2544

[71] Carter-Fenk K., Johnson B.A., Herbert J.M., Schenter G.K., Mundy C.J., Birth of the hydrated electron via charge-transfer-to-solvent excitation of aqueous iodide, *J. Phys. Chem. Lett.*, **14** (2023), 870–878

[72] Lan J.G., Rybkin V.V., Pasquarello A., Temperature-dependent properties of the aqueous electron, *Angew. Chem. Int. Ed.*, **61** (2022), e202209398

[73] Ambrosio F., Miceli G., Pasquarello A., Structural, dynamical and electronic properties of liquid water: a hybrid-functional study, *J. Phys. Chem. B*, **120** (2016), 7456–7470

[74] Ambrosio F., Miceli G., Pasquarello A., Redox levels in aqueous solution: effect of van der Waals interactions and hybrid functionals, *J. Chem. Phys.*, **143** (2015), 244508

[75] Sabatini R., Gorni T., de Gironcoli S., Non-local van-der-Waals density functional made simple and efficient, *Phys. Rev. B*, **87** (2013), 041108

[76] Vydrov O.A., Van Voorhis T., Non-local van-der-Waals density functional: the simpler the better, *J. Chem. Phys.*, **133** (2010), 244103

[77] Lippert G., Hutter J., Parrinello M., A hybrid Gaussian and plane-wave density-functional scheme, *Mol. Phys.*, **92** (1997), 477–487

[78] Dunning T.H., Gaussian basis sets for use in correlated molecular calculations. I. The atoms boron through neon and hydrogen, *J. Chem. Phys.*, **90** (1989), 1007–1023

[79] Guidon M., Hutter J., VandeVondele J., Auxiliary density-matrix methods for Hartree–Fock exchange calculations, *J. Chem. Theory Comput.*, **6** (2010), 2348–2364

[80] Bussi G., Donadio D., Parrinello M., Canonical sampling through velocity rescaling, *J. Chem. Phys.*, **126** (2007), 014101

[81] Bl"ochl P.E., Electrostatic decoupling of periodic images of plane-wave-expanded densities and derived atomic point charges, *J. Chem. Phys.*, **103** (1995), 7422–7428

[82] Laino T., Mohamed F., Laio A., Parrinello M., An efficient linear-scaling electrostatic coupling for treating periodic boundary conditions in QM/MM simulations, *J. Chem. Theory Comput.*, **2** (2006), 1370–1378

[83] Lu T., Chen F., Multiwfn: a multifunctional wavefunction analyser, *J. Comput. Chem.*, **33** (2012), 580–592

[84] Humphrey W., Dalke A., Schulten K., VMD: visual molecular dynamics, *J. Mol. Graph.*, **14** (1996), 33–38

[85] Chen M., Ko H.Y., Remsing R.C., Calegari-Andrade M.F., Santra B., Sun Z., Selloni A., Car R., Klein M.L., Perdew J.P., Wu X., *Ab initio* theory and modelling of water, *Proc. Natl. Acad. Sci.*, **114** (2017), 10846–10851

[86] Wen B., Selloni A., Hydrogen bonds and H_3O^+ formation at the water interface with formic-acid-covered anatase TiO_2, *J. Phys. Chem. Lett.*, **12** (2021), 6840–6846

[87] Widmer D.R., Schwartz B.J., Solvents can control solute molecular identity, *Nat. Chem.*, **10** (2018), 910–917

[88] Jacobson L.D., Herbert J.M., Theoretical characterisation of four distinct isomer types in hydrated-electron clusters, and proposed assignments for photoelectron spectra of water-cluster anions, *J. Am. Chem. Soc.*, **133** (2011), 19889–19899

[89] Meng X., Guo J., Peng J., Chen J., Wang Z., Shi J.R., Li X.Z., Wang E.G., Jiang Y., Direct visualisation of concerted proton tunnelling in a water nanocluster, *Nat. Phys.*, **11** (2015), 235–239

[90] Peng J., Cao D., He Z., Guo J., Hapala P., Ma R., Cheng B., Chen J., Xie W.J., Li X.Z., Jel'inek P., Xu L.M., Gao Y.Q., Wang E.G., Jiang Y., The effect of hydration number on the interfacial transport of sodium ions, *Nature*, **557** (2018), 701–705

[91] Otlyotov A.A., Itkis D., Yashina L.V., Cavallo L., Minenkov Y., Physical and numerical aspects of sodium-ion solvation free energies via the cluster–continuum model, *Phys. Chem. Chem. Phys.*, **24** (2022), 29927–29939

[92] Burnham C.J., Petersen M.K., Day T.J.F., Iyengar S.S., Voth G.A., The properties of ion–water clusters. II. Solvation structures of Na^+, Cl^- and H^+ clusters as a function of temperature, *J. Chem. Phys.*, **124** (2006), 024327

[93] Marin T.W., Takahashi K., Jonah C.D., Chemerisov S.D., Bartels D.M., Recombination of the hydrated electron at high temperature and pressure in hydrogenated alkaline water, *J. Phys. Chem. A*, **111** (2007), 11540–11551

[94] Bai C., Herzfeld J., Special pairs are decisive in the auto-ionisation and recombination of water, *J. Phys. Chem. B*, **121** (2017), 4213–4219

[95] Buxton G.V., Greenstock C.L., Helman W.P., Ross A.B., Critical review of rate constants for reactions of hydrated electrons, hydrogen atoms and hydroxyl radicals ($\cdot OH/\cdot O^-$) in aqueous solution, *J. Phys. Chem. Ref. Data*, **17** (1988), 513–886

[96] Han P., Bartels D. M., Hydrogen/deuterium isotope effects in water radiolysis. 4. the mechanism of aquated Haq $\rightleftharpoons$ (e)aq interconversion, *J. Phys. Chem.*, **96** (1992), 4899-4906

[97] Barnett R.N., Giniger R., Cheshnovsky O., Landman U., Dielectron attachment and hydrogen-evolution reaction in water clusters, *J. Phys. Chem. A*, **115** (2011), 7378–7391

[98] Li M., Wang P., Yu X., Su Y., Zhao J., Impact of nuclear-quantum effects on the structural properties of protonated water clusters, *J. Phys. Chem. A*, **128** (2024), 5954–5962

[99] Warburton R. E., Soudackov A. V., Hammes-Schiffer S. A., Theoretical modeling of electrochemical proton-coupled electron transfer, *Chem. Rev.*, **122** (2022), 10599-10650